Dossier

This paper is a part of the hereunder thematic dossier published in OGST Journal, Vol. 68, No. 2, pp. 187-396 and available online here

Cet article fait partie du dossier thématique ci-dessous publié dans la revue OGST, Vol. 68, n°2, pp. 187-396 et téléchargeable ici

DOSSIER Edited by/Sous la direction de : **Jean-Charles de Hemptinne**

InMoTher 2012: Industrial Use of Molecular Thermodynamics
InMoTher 2012 : Application industrielle de la thermodynamique moléculaire

Oil & Gas Science and Technology – Rev. IFP Energies nouvelles, Vol. 68 (2013), No. 2, pp. 187-396

IFP Energies nouvelles

Oil & Gas Science and Technology – Rev. IFP Energies nouvelles, Vol. 68 (2013), No. 2, pp. 299-307

DOI: 10.2516/ogst/2012042

Dossier

InMoTher 2012 - Industrial Use of Molecular Thermodynamics
InMoTher 2012 - Application industrielle de la thermodynamique moléculaire

Isotherms of Fluids in Native and Defective Zeolite and Alumino-Phosphate Crystals: Monte-Carlo Simulations with "On-the-Fly" *ab initio* Electrostatic Potential

X. Rozanska*, P. Ungerer, B. Leblanc and M. Yiannourakou

Materials Design, 18 rue de Saisset, 92120 Montrouge - France
e-mail: xrozanska@materialsdesign.com - pungerer@materialsdesign.com - bleblanc@materialsdesign.com - myiannourakou@materialsdesign.com

* Corresponding author

Résumé — Isothermes d'adsorption de fluides dans des zéolithes silicées et dans des cristaux alumino-phosphatés : simulations de Monte Carlo utilisant un potentiel électrostatique *ab initio* — Nous utilisons la théorie de la fonctionnelle de la densité (DFT en anglais) pour engendrer le potentiel électrostatique en tout point de la microporosité de matériaux adsorbants et nous utilisons cette information pour modéliser l'adsorption par simulation de Monte Carlo dans l'ensemble Grand Canonique. Ceci nous permet de simuler des solides complexes montrant des défauts, sans qu'il soit nécessaire de définir *a priori* leurs paramètres électrostatiques. Nous appliquons cette méthode aux aluminophosphates et silicates cristallins microporeux de type ZON et nous évaluons les sélectivités d'adsorption et séparation dans des systèmes CO_2-N_2 ou CO_2-H_2O.

Abstract* — *Isotherms of Fluids in Native and Defective Zeolite and Alumino-Phosphate Crystals: Monte-Carlo Simulations with "On-the-Fly"* Ab Initio *Electrostatic Potential — *We use periodic Density Functional Theory (DFT) method to generate the electrostatic potentials of adsorption materials and use them in Grand Canonical Monte Carlo simulations of fluid adsorption isotherms. This permits us to consider complex solids showing defects and without* a priori *knowledge of their electrostatic parameters for the Monte Carlo simulations. We apply the method to aluminophosphate and silicate solids of ZON type and evaluate their affinity to adsorb and separate CO_2-N_2(H_2O) mixtures.*

INTRODUCTION

Molecular mechanics methods have shown their efficiency at complementing and further validating experimental adsorption data of fluids in microporous solids [1, 2]. However, the determination of the forcefield parameters that are used to compute the guest-host potential energy can be a difficult and time consuming process, especially for the parameters describing the electrostatic interactions. To overcome these difficulties, the electrostatic potential of the solid into which the fluid adsorbs can directly be used from periodic *ab initio* calculation [3]. This operation is done in a single step and only requires the solid crystal atomic positions. Another huge benefit of this approach is its versatility: there are virtually no limitations related to the solid crystal structure and the presence of defects in it (apart its size, which should be around several hundred atoms). To illustrate the strength and elegance of this approach, we consider the case of silicate and aluminophosphate crystals and the inclusion of silica defects in them, compensated or not by Na^+. The CO_2, N_2 and H_2O isotherms in the native and defective crystal structures are determined and compared. The case of the CO_2-N_2 mixtures

isotherms is then investigated. Aluminophosphates (ALPO) have been shown to be interesting materials to separate CO_2 from CO_2-N_2 mixtures as obtained from flue gas [4]. CO_2 separated from the mixture can afterwards be sequestered in geological deposits [5].

1 METHODS AND MODELS

1.1 Solid Models

The starting ZON coordinates were taken from Roux *et al.* [6]. ZON has networks of parallel and zig-zag 8-membered ring micropores that interconnect and a zig-zag 6-membered ring network that also interconnects the large parallel network *(Fig. 1)* [7]. The symmetry group of ZON (1 and 2) is PBCA (orthorhombic+D_{2h} axis). The all silica equivalent is obtained by substituting all Al and P with Si. The silica defect ALPO models are defined by substituting twice adjacent Al-P pair (*Fig. 1c*) and a P atom (*Fig. 1d*). We sampled the different possible sites of Al-P pair substitution with Si-Si and computed their energies using MOPAC [8]. We selected the most energetically stable site. For material 4 *(Tab.1)*, the electroneutrality of the system is verified after addition of Na^+ near the Si-defect and in the parallel 8-membered ring micropore *(Fig. 1)*. Because the substitution of an Al-P pair with Si-Si pair does not change the global charge of the solid, charge compensating anion or cation is not needed. The introduction of defect in the ZON periodic unit cell lowers its symmetry group and the symmetry group is lowered to P1 for 3 and 4. Therefore, symmetry group P1 is used for all systems, including 1 and 2.

1.2 Periodic Density Functional Theory Calculations

The periodic DFT code VASP (Vienna Ab-initio Simulation Package) [9, 10] is used to optimize the cell size and shape as well as all atomic positions with the only constraint that the cell symmetry remains orthorhombic, *i.e.*, $\alpha = \beta = \gamma = 90°$. The geometry optimizations are done using the conjugate gradient method as implemented in VASP-MedeA (Materials Exploration and Design Analysis) v. 4.6. The criteria to end the geometry optimization are considered met when all forces acting on atoms are less than 0.0193 $kJ.mol^{-1}.pm^{-1}$ (0.02 $eV.Å^{-1}$). The DFT functional that is used in the energy and force calculations is PBE [11, 12] together with the Projected Augmented Wave (PAW) approach [13, 14]. An energy cutoff of 38.596 $MJ.mol^{-1}$ (400 eV) is set for the electronic wave functions. The optimized parameters of the cells are given in Table 1. After the cells are optimized, the total electrostatic potential calculations are done and the obtained electrostatic potential VASP files are converted to the format of the Monte Carlo code Gibbs without further modification.

1.3 Molecular Mechanic Monte-Carlo Simulations

All isotherm calculations are done using the Monte-Carlo code Gibbs v. 9.2 [15] as implemented in MedeA v. 2.8 [16].

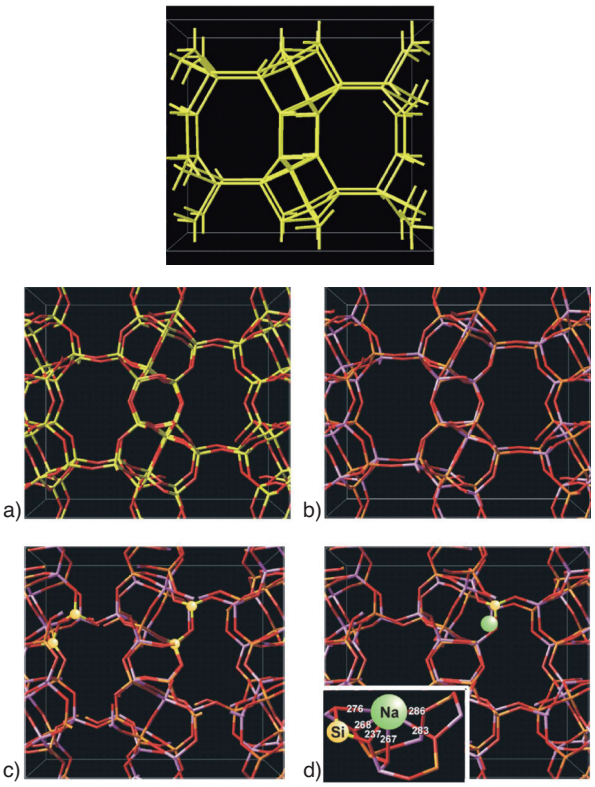

Figure 1

Details of the ZON Structures: a) SiO_2, b) $AlPO_4$, c) $Al_{30}Si^4P_{30}O_{128}$, d) $NaAl^{32}SiP_{31}O_{128}$. The bond distances in the inset of d) are in pm.

TABLE 1

Optimized composition, geometry and energy of the ZON solids[a]

Composition	Label	Cell size	Total volume	Porosity[b]
$Si_{64}O_{128}$	1	1 379 × 1 492 × 1 710	3.52	0.28
$Al_{32}P_{32}O_{128}$	2	1 379 × 1 491 × 1 710	3.52	0.20
$Al_{30}Si_4P_{30}O_{128}$	3	1 329 × 1 446 × 1 621	3.12	0.13
$NaAl_{32}SiP_{31}O_{128}$	4	1 353 × 1 463 × 1 677	3.32	0.16

[a] The $a \times b \times c$ vector lengths of the cell size and total cell volume are given in pm × pm × pm and nm^3, respectively.
[b] The porosity is the micropore volume as determined by Monte-Carlo simulated He-pycnometry (see next section) divided by the total volume of the cell.

Rigid molecule model is used for the fluid molecules, namely N_2, CO_2 and H_2O, in their pure or mixture state. For N_2 and CO_2, the Lennard-Jones parameters, charges and geometries as given from the database of MedeA are used [17, 18]. Water is modeled using the TIP3P model from Jorgensen *et al.* (1983) [18, 20]. Its simulated saturation pressure is measured to be 27 mbar while the experimental value is 32 mbar at 298 K [19].

For the adsorption isotherm simulations of fluid on a solid, the solid is assumed rigid in the Gibbs code and Lennard-Jones and electrostatic potential energy grids characterizing the solid are generated prior the Monte-Carlo sampling tasks take place. The grids were generated for 2 × 2 × 2 extension of the primitive cells, *i.e.*, the grid dimensions are ca. 2.8 × 3.0 × 3.4 nm^3. In accord with previous results [20], only oxygen atom parameters are considered to generate the solid Lennard-Jones potential energy grid. The Lennard-Jones parameters for aluminophosphates [21, 24] and silicates [22] oxygen atoms are different yet defined from the same group for consistency. They have been validated *vs* experimental data of alkanes and water adsorption isotherms [21-27].

All Monte-Carlo simulation runs are done in the Grand Canonical ensemble [24] at T = 298 K. For every simulation of a given fluid composition (pure or mixture) and fugacity, an equilibration run of five million steps takes place prior a production run of twenty five million steps. To ease the Monte-Carlo sampling, a configurational bias is used [25]. The Lennard-Jones pair energy cutoff is set to 2 nm, while the electrostatic potential energy is evaluated *via* Ewald summation, the optimal Ewald summation parameters being set automatically [30].

Prior to the determination the adsorption isotherms of N_2, CO_2, H_2O and their mixtures, we determine the micropore volume to compute the solid porosity. This is done by helium-pycnometry simulations at low fugacity (0.001, 0.01 and 0.1 bar). At these low fugacities, helium behaves like an ideal gas and the density of helium in the solid is considered to be the same than that of bulk helium under the same conditions of fugacity and temperature. Hence, the determinations of the amount of helium adsorbed in the solid and of the bulk helium density give a direct estimate of the pore volume. Bulk helium density is determined by Grand Canonical Monte-Carlo simulation using the same temperature and fugacity than that used in the helium adsorption on the solids. The pore volume divided by the total solid volume gives the solid porosity. The porosities are reported in Table 1.

The water isotherm data are total number of adsorbed molecules, while that of N_2 and CO_2 are Gibbs excess adsorption values. The molecular excess adsorption is defined as:

$$n_{ex} = n_{tot} - n_{id} \quad (1)$$

where n_{tot} is the total number of molecules adsorbed on the solid at a given fugacity and composition in a given solid volume and n_{id}, the number of molecule, non-interacting with the solid at the same fugacity and composition and in a volume equals to that of the micropore volume of the solid as determined by simulated helium-pycnometry. The n_{id} values are determined using the same protocol than that used to determine the ideal helium density in the simulated helium-pycnometry. The excess adsorption values, N_{ex}, are then expressed in $g.cm^{-3}$ following:

$$N_{ex} = n_{ex}\, M\, V_s^{-1}\, N_A^{-1} \quad (2)$$

where M is the mole mass of the considered fluid ($g.mol^{-1}$), V_s the total volume of the solid for which n_{ex} is measured (m^3) and N_A the Avogadro number (mol^{-1}).

2 RESULTS AND DISCUSSION

2.1 Influence of the Lennard-Jones and Electrostatic Potential on the Adsorption Isotherms of N_2

We consider the case of $AlPO_4$ and SiO_2 ZON frameworks before to simulate the adsorption of pure compound and mixtures of H_2O, N_2 and CO_2 in the defective ZON solids. We limit the adsorption isotherm simulations to N_2 and analyze the consequences of changing the electrostatic and Lennard-Jones parameters. We calculate the Gibbs excess adsorption of N_2 between 1 and 120 bar and the isosteric heats of N_2 adsorption on the solids between 1 mbar and 1 bar using the $AlPO_4$ and SiO_2 frameworks, silicate and aluminophosphate Lennard-Jones oxygen parameters and electrostatic potential grids obtained from "classical" point charges [21, 24, 23, 27] and *ab initio* calculations using VASP. The Lennard-Jones

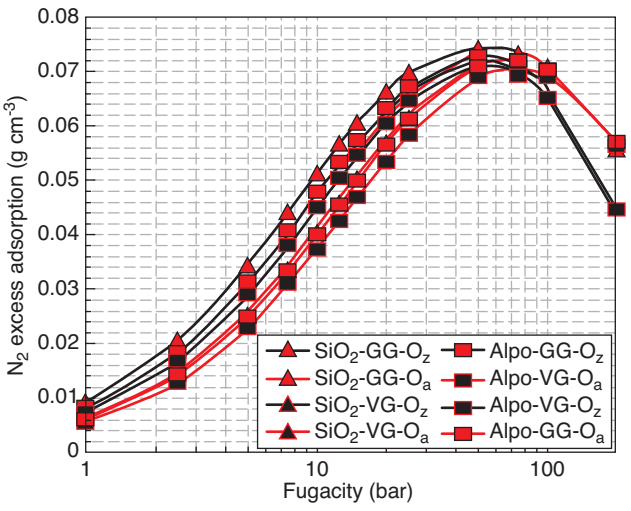

Figure 2

Influence of the Lennard-Jones and electrostatic potential parameters on the simulated (Gibbs excess) adsorption isotherms of N_2 in SiO_2 and $AlPO_4$-ZON for N_2 fugacities between 1 and 120 bar. The designation of the curves is done as follow: SiO_2 and Alpo are for SiO_2 and $AlPO_4$ atomic positions, respectively, GG and VG are for point charges and *ab initio* electrostatic potentials, respectively and O_z and O_a are for silicate and aluminophosphate Lennard-Jones potentials, respectively.

parameters for silicate and aluminophosphate oxygen atoms are 517.6 and 779.4 J.mol^{-1} for ε and 347.3 and 300 pm for σ, respectively. The adsorption isotherms and heats are given in Figure 2 and Table 2, respectively.

TABLE 2

Influence of the Lennard-Jones and electrostatic potential parameters on the simulated isosteric heat of adsorption of N_2 in SiO_2 and $AlPO_4$-ZON for N_2 fugacities between 1 mbar and 1 bar[a]

Structure-electrostatic potential	O_z	O_a
SiO_2-point charge	17.4	18.4
SiO_2-*ab initio*	16.8	17.8
$AlPO_4$-point charge	17.3	18.2
$AlPO_4$-*ab initio*	16.8	17.7

[a] All the values are in kJ.mol^{-1}. O_z and O_a are for silicate and aluminophosphate oxygen atom Lennard-Jones parameters, respectively.

The atomic positions in the systems lead to similar adsorption heat values and adsorption isotherms. For instance, the heats of adsorption change by 0.2 kJ.mol^{-1} at maximum. The other parameters have a more important weight. Switching from silicate to aluminophosphate oxygen Lennard-Jones parameters changes the isosteric heats of adsorption of N_2 by ca. 1.0 kJ.mol^{-1}. The point charge and *ab initio* electrostatic potentials change the heats of adsorption by ca. 0.6 kJ.mol^{-1}. The point charge electrostatic potentials show higher heats of adsorption than that obtained with *ab initio* electrostatic potentials.

For the eight possible combinations of systems, Lennard-Jones and electrostatic potential parameters reveal common trends and features when the N_2 Gibbs excess adsorption isotherm data are analyzed *(Fig. 2)*. The N_2 excess adsorption increases with N_2 fugacity before to drop above ca. 40-50 bar. The values remain positive in the considered range (*i.e.*, 10^{-3} to 200 bar). As also pointed out by the isosteric heat of adsorption, the Lennard-Jones parameters are the dominant ones. This is clearly seen at 200 bar when all curves end up in two. The largest amount of N_2 is obtained for adsorption in materials that use aluminophosphate oxygen Lennard-Jones parameters. At low or moderate fugacity, the trend is also well marked: the amount of adsorbed N_2 is lower in systems defined with aluminophosphate oxygen Lennard-Jones parameters than with silicate ones. Although the electrostatic potential parameter is not the dominant in the case of the adsorption of N_2, it plays a role and alters the adsorption isotherms *(Fig. 2)*. The importance and influence of atomic charges on adsorption isotherms has been observed before in simulations [3, 27-29]. At high fugacity, there is practically no effect of the electrostatic potential as mentioned previously. At low and moderate N_2 fugacity, the amount of N_2 is always larger when a point charge electrostatic potential is used.

2.2 N_2 Adsorption Isotherms and Isosteric Heats in ZON-Type Materials

Now, we consider the adsorption of N_2 from fugacity of 10^{-3} to 200 bar in materials 1, 2, 3 and 4. The Monte-Carlo simulations data are shown in Figure 3. The Gibbs excess sorption of N_2 increases in all solids before to reach a maximum at fugacity between 50 and 200 bar. The maxima are reached at 50 bar in 1 and ca. 75 bar in 2. When defects are present, the maxima are reached at higher fugacities: the maxima are reached at 100 and 200 bar in 4 and 3, respectively. The N_2 fugacity at which the Gibbs excess sorption maxima are reached follows the same ordering than that of the ZON porosity or micropore volume *(Tab. 1)*. If we project the micropore volume into a hypothetical single cylinder contained in the solid unit cell, the diameters for 1, 2, 3 and 4 are 910, 760, 590 and 670 pm, respectively.

To a large extent, the isosteric heats of adsorption of N_2 are constants in a given solid. It is only at N_2 fugacity close to that of the fluid condensation that they, first, increase slightly before a large drop. The small maxima in the adsorption heats do not exactly take place at the same fugacity than that of the Gibbs excess sorption *(Fig. 3)*. The heats between 10^{-3} to ca. 1 bar are approximately constant and equal to 16.8, 17.7, 18.4 and 18.8 kJ.mol^{-1} for 1, 2, 3 and 4, respectively. To compute the Gibbs excess sorption, we performed the Grand Canonical simulation of N_2 alone. This simulation gives us the isosteric heat of N_2 as function of fugacity: it is equal to 2.5 kJ.mol^{-1} up to ca. 10 bar and then increases up to 4.5 kJ.mol^{-1} at 200 bar. This does not provide support to better interpret or analyze the evolution of the isosteric heat of adsorption of N_2 in 1, 2, 3 and 4 as a function of the fugacity. The zero-pressure extrapolation heat of adsorption of N_2 in silicalite is experimentally reported to be 17.6 kJ.mol^{-1} [30]. We did not sample higher pressure than 200 bar but the behavior observed for 1 with N_2 fugacity beyond the adsorption heat maximum is likely to be equivalent for 2, 3 and 4.

2.3 CO_2 Adsorption Isotherms and Isosteric Heats in ZON-Type Materials

The Gibbs excess and isosteric heat of adsorption of CO_2 in the ZON materials obtained from the Monte-Carlo simulation are reported in Figure 4.

The Gibbs excess sorption isotherms of CO_2 in 1, 2, 3 and 4 increase before they drop between 25 and 50 bar when CO_2 becomes liquid. The experimental partial pressure of CO_2 is 64.3 bar at 298 K [31]. The maximum value that is reached in 1 is larger than those in 2, 3 and 4, which are all three rather close. After condensation of CO_2 took place in the pores above 50 bar, the adsorption curves show equivalent slopes although they are shifted with respect to each other. At 200 bar, the adsorbed CO_2 amount is -0.05 g.cm^{-3} in 1 and 2, 0.04 g.cm^{-3} in 3 and -0.01 g.cm^{-3} in 4. We did not investigate

adsorption above 200 bar but the curve slopes suggest that Gibbs excess sorption becomes negative in all solids.

The isosteric heats of adsorption of CO_2 in the different solids are again practically constant when the CO_2 fugacity is below 1 bar. The heats are 25.4, 27.0, 30.9 and 28.6 kJ.mol^{-1}, in 1, 2, 3 and 4, respectively, while the experimental heat of adsorption in silicalite is 27.2 kJ.mol^{-1} [30]. Above 1 bar, the heats of adsorption in 1 and 4 increase up to the value in 3, which remains at similar value than that at low fugacity. The heat in 2 increases by 0.5 kJ.mol^{-1} between 5 and 20 bar and, then, drops down to 24.7 kJ.mol^{-1} at 200 bar. The isosteric heat of pure CO_2 in the absence of solid is practically constant up to 30 bar and equal to 2.5 kJ.mol^{-1} and then it increases up to 27 kJ.mol^{-1} at 200 bar. This does not help to interpret or analyze the evolution of the isosteric heat of adsorption of CO_2 in 1, 2, 3 and 4 as a function of the fugacity.

The isosteric heats of adsorption of CO_2 and N_2 and especially their variations as a function of the fluid fugacity are qualitatively distinct. The heat of adsorption is practically unchanged for N_2 in the range 10^{-3}-200 bar in 2, 3 and 4 and shows a drop above 50 bar in 1. In the case of CO_2, only the adsorption heat in 3 remains practically unchanged. The heat of adsorption in 1 and 4 increases and it is in 2 that it drops at high fugacity.

2.4 H_2O Adsorption Isotherms in ZON-Type Materials

$AlPO_4$ and SiO_2 microporous crystals are hydrophobic materials [32], the latter being less hydrophobic than the former. However, less is known when defects are present, although ion-exchanged zeolites and aluminophosphate crystals show increasing hydrophilicity with the amount of ions in the structure [32]. We analyze the water adsorption isotherms in our ZON models by means of Grand Canonical Monte-Carlo simulations. The results are shown in Figure 5: we report the total amount of adsorbed water per volume of solid in the inset graph, while the data are expressed per micropore volume of solid in the main graph.

The ZON micropore saturation with water occurs at higher fugacity than in the case of water alone, which takes place at 27 mbar for our water model. In our solids, the condensation of water is obtained between 0.1 and 0.4 bar in 1 and between

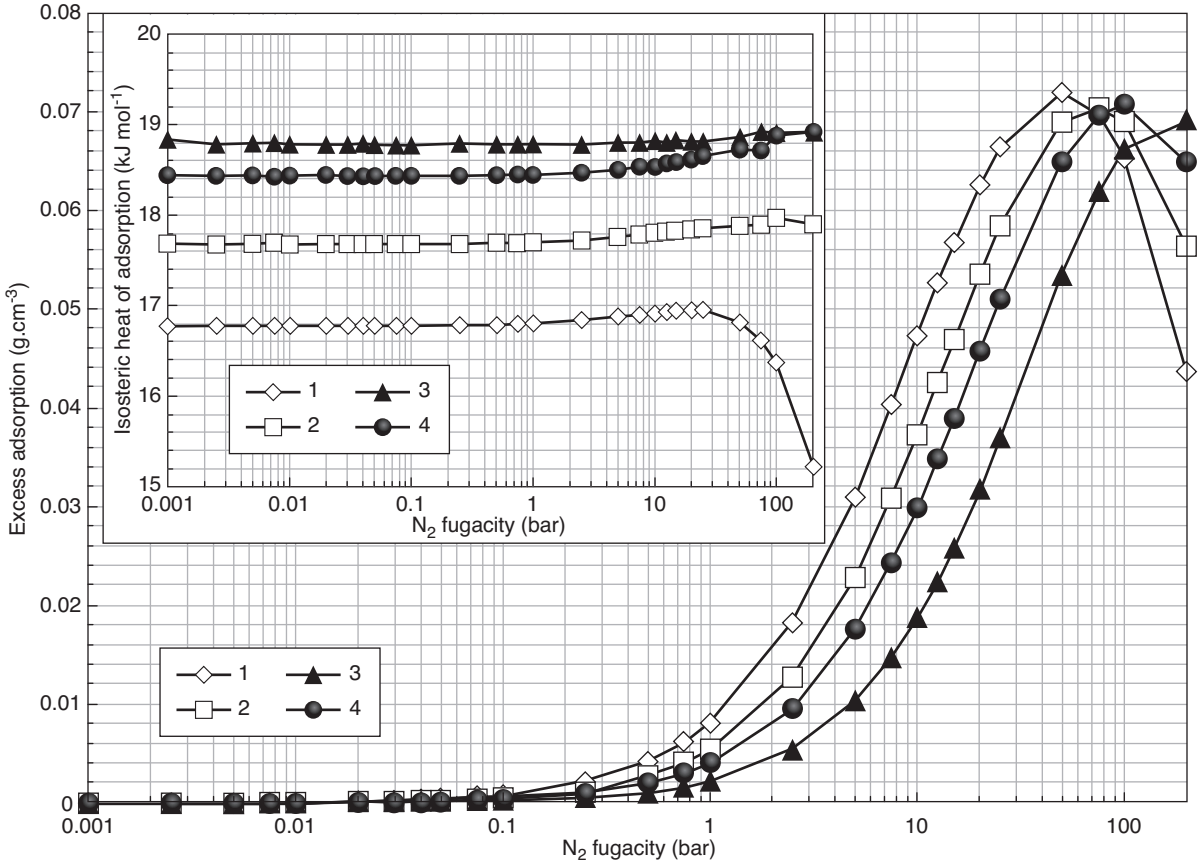

Figure 3

Excess adsorption isotherms and isosteric heats of adsorption (inset) of N_2 in ZON-type materials.

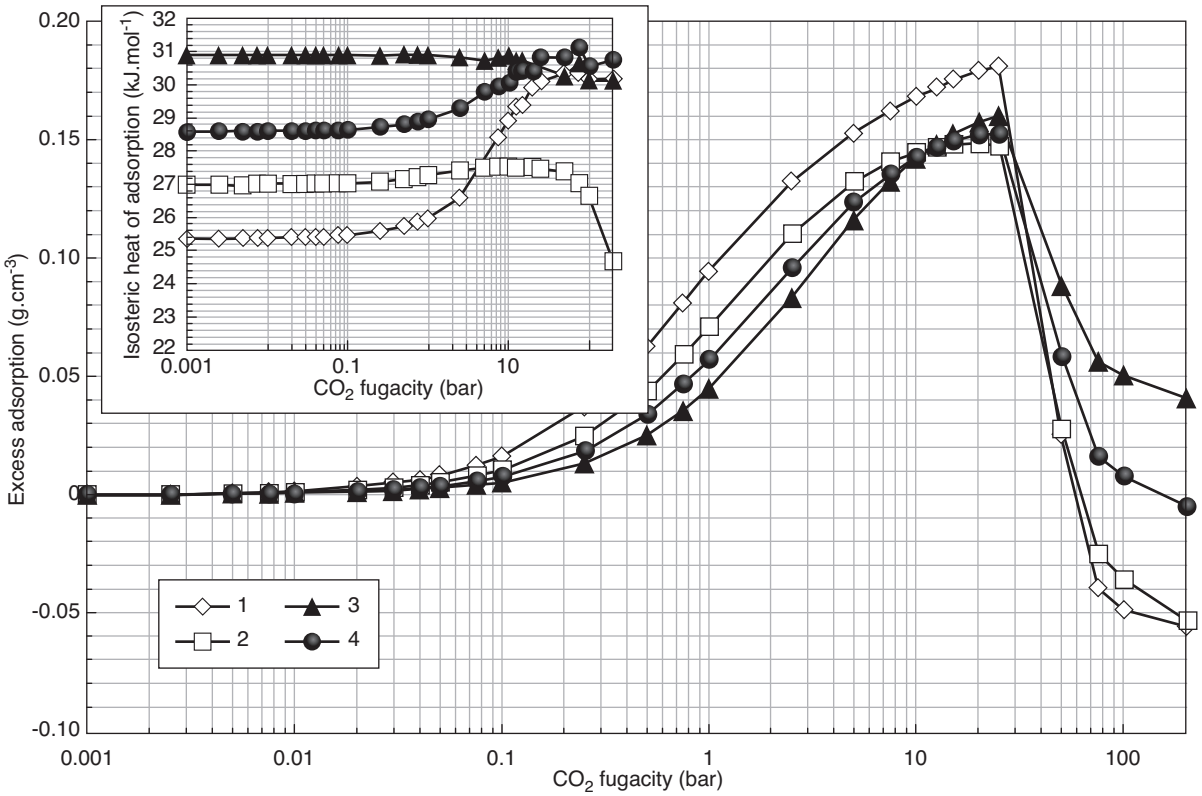

Figure 4

Excess adsorption isotherms and isosteric heats of adsorption (inset) of CO_2 in ZON-type materials.

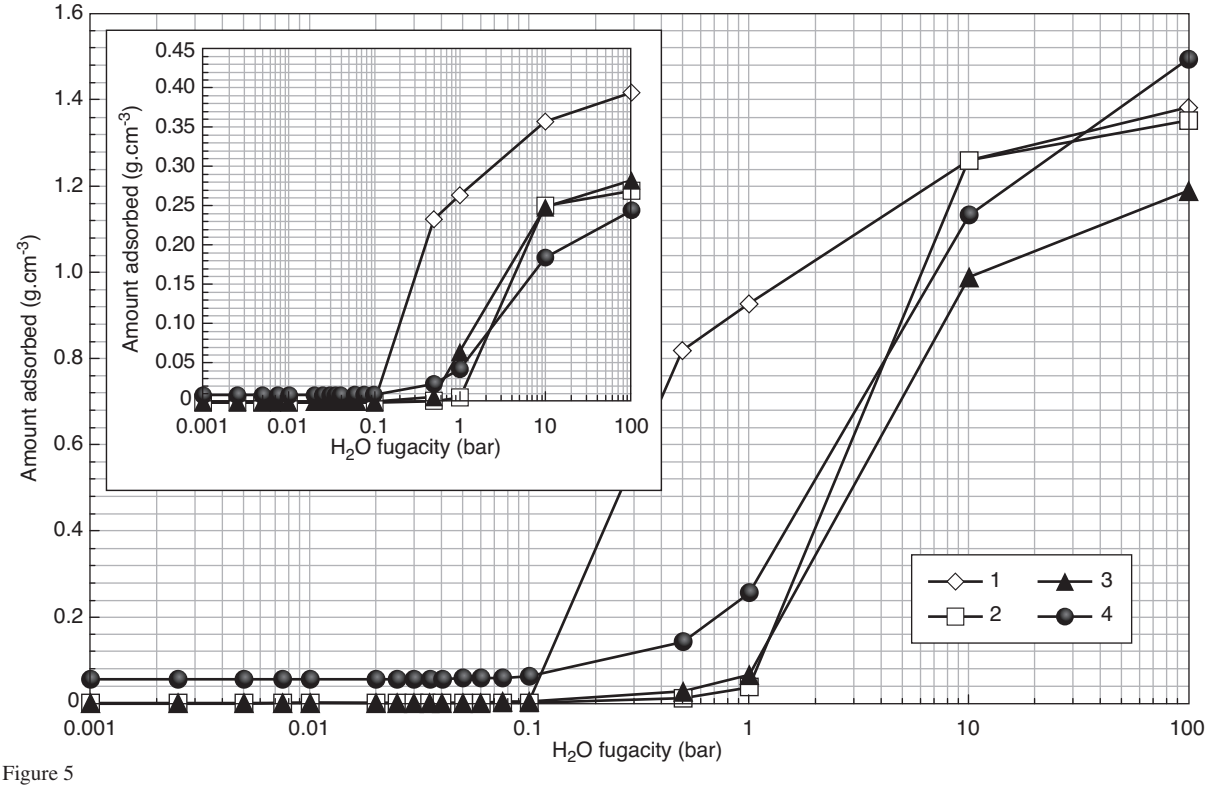

Figure 5

Adsorption isotherms of H_2O in ZON-type materials.

1 and 10 bar in 2, 3 and 4. This is well above the water saturation pressure at 298 K. Hence, "wet" gases should not lead to the water filling of the solid micropores here. However, 4 shows a different water isotherm than the other solids. Even at extremely low water fugacity (1 mbar), a water molecule binds to the solid: inspection of the conformations generated by Monte-Carlo simulations reveals that this water molecule is always found in the vicinity of Na^+. Unless the driest conditions are met, it seems experimentally impossible to avoid presence of this water molecule and the stoichiometric formula of 4 is better considered as $[H_2O{\bullet}NaAl_{32}SiP_{31}O_{128}]$. The amount of water in 1, 2 and 3 remains negligible below ca. 0.1 bar.

2.5 Adsorption Isotherms of "Wet" CO_2-N_2 Mixture in ZON-Type Materials

Now, we focus on the results obtained on the Monte-Carlo simulations of the adsorption of CO_2-N_2 mixtures *(Fig. 6)*. We analyzed the water adsorption and observed that water is present in 4 and can be considered absent in 1, 2 and 3. For the adsorption of CO_2-N_2 in 4, we set a "residual" H_2O fugacity of 1 mbar and obtained in all simulation a water molecule present near Na^+. We determine the CO_2/N_2 molecular ratio as a function of fugacity in an empty cell by Grand Canonical Monte-Carlo simulations. The values are reported in the inset graph in Figure 6. Between 1 and ca. 30 bar, the CO_2/N_2 ratio remains constant and equals to 1: CO_2 and N_2 behave like ideal gases. Between 50 and 80 bar, CO_2 condensates and the CO_2/N_2 ratio becomes larger than 1. The values in the main graph in Figure 6 are normalized with the ratio values of the inset graph. The fugacity values in the *x*-axis are the sum of the CO_2 and N_2 fugacities, which are equal.

There are more than ten times more CO_2 molecules adsorbed in the ZON micropores than N_2 molecules. This can be explained by the larger isosteric heat of adsorption of CO_2 than that of N_2 in the solids *(Fig. 3, 4)*. In all solids, the CO_2/N_2 ratio drops gradually above 10 bar and the ratios are around 3 in 2, 3, 4 and 5 in 1 at 100 bar. For all systems except 1, the ratios have an increasingly negative slope as a function of the fugacity. The case of 1 is different: the CO_2/N_2 ratio actually increases between 1 and ca. 30 bar and drops at higher fugacity. The molecular ratios and their evolution as a function of the fugacity are practically equivalent in 2 and 4. The material that shows the highest affinity for CO_2 at 1 bar is 3, with a CO_2/N_2 ratio of 15, while it is 13 in 1 and 12 in 2 and 4. Above 10 bar and because of the positive

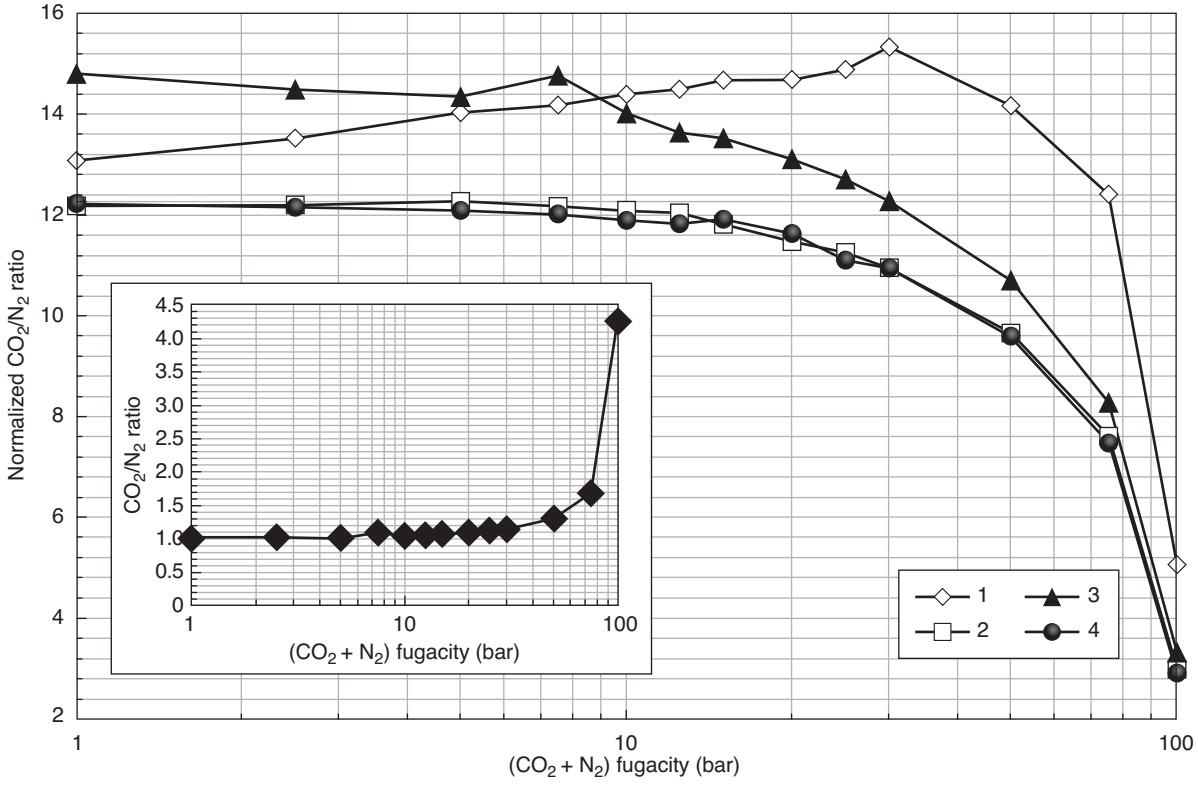

Figure 6

Molecular CO_2/N_2 ratio from the adsorption isotherms of CO_2 and N_2 in ZON-type materials.

slope of CO_2/N_2 ratio in 1, CO_2 shows the highest affinity in 1. The highest CO_2 affinity in 1 is reached at 30 bar and then it lowers when CO_2 starts to condensate in the micropores.

The CO_2 and N_2 adsorption competition in the ZON micropores is difficult to estimate *a priori* from the adsorption of the pure fluids. The adsorption isotherm simulations of the binary (ternary with H_2O) mixture appear mandatory to get an estimate of the CO_2 *versus* N_2 adsorption affinity in the solids. In the current work, we did not analyze time-dependent properties, which are also required to get a complete estimation of the separation properties of fluids by solids [33, 34]. The Monte-Carlo formalism is not the most appropriate to simulate these and dynamic molecular simulations would be required to complement the evaluation of the separation properties of the above materials. However, due to the large similarities between the solid structures, it is likely that the diffusion constants in the different materials should not be very different.

CONCLUSION

We have shown that an intimate coupling of periodic DFT and MM Monte-Carlo methods is possible and permits to describe complex systems. Integration of periodic DFT and molecular mechanic methods in our chemical simulation interface MedeA permits to prepare and submit large number of calculations and to easily analyze them. The periodic DFT calculations give rigorous and unambiguous parameters that can be used directly in the molecular simulations. The bottleneck of the availability of forcefield parameters for the simulations is strongly reduced. The application of this approach to the separation of CO_2/N_2 mixtures in presence of water by solids illustrates its sensitivity and elegance and its high chemical engineering interest. The simulations reveal that ZON with chemical composition $Al_{15}Si_2P_{15}O_{64}$ is the material that shows the largest affinity for CO_2 adsorption below 10 bar. At higher fugacity, ZON with chemical composition SiO_2 becomes more suitable material to adsorb favorably CO_2.

REFERENCES

1 Pascual P., Ungerer P., Tavitian B., Pernot P., Boutin A. (2003) Development of a Transferable Guest-host Force Field for Adsorption of Hydrocarbons in Zeolites I. Reinvestigation of Alkane Adsorption in Silicalite by Grand Canonical Monte Carlo Simulation, *Phys. Chem. Chem. Phys.* **5**, 17, 3684-3693.

2 Wender A., Barreau A., Lefebvre C., Di Lella A., Boutin A., Ungerer P., Fuchs A.H. (2007) Adsorption of *n*-Alkanes in Faujasite Zeolites: Molecular Simulation Study and Experimental Measurements, *Adsorption* **13**, 5-6, 439-451.

3 Watanabe T., Manz T.A., Sholl D.S. (2011) Accurate Treatment of Electrostatics during Molecular Adsorption in Nanoporous Crystals without Assigning Point Charges to Framework Atoms, *J. Phys. Chem. C* **115**, 11, 4824-4836.

4 Li S., Fan C.Q. (2010) High-Flux SAPO-34 Membrane for CO_2/N_2 Separation, *Ind. Eng. Chem. Res.* **49**, 9, 4399-4404.

5 Mazumder S., Van Hemert P., Busch A., Wolf K.-H.A.A., Tejera-Cuesta P. (2006) Flue Gas and Pure CO_2 Sorption Properties of Coal: A Comparative Study, *Int. J. Coal Geol.* **67**, 267-279.

6 Roux M., Marichal C., Le Meins J.-M., Baerlocher C., Chézeau J.-M. (2003) Solid State NMR and X-ray Diffraction Study of Three Forms of the Aluminophosphate $AlPO_4$-ZON, *Micropor. Mesopor. Mater.* **63**, 1-3, 163-176.

7 Bailly A., Amoureux J.P., Wiench J.W., Pruski M. (2001) Structural Analysis of ZON-Type Aluminophosphates by Solid State NMR, *J. Phys. Chem. B* **105**, 4, 773-776.

8 MOPAC2009, Stewart J.J.P., Stewart Computational Chemistry, Colorado Springs, CO, USA, http://OpenMOPAC.net (2008).

9 Kresse G., Furthmüller J. (1993) *Ab Initio* Molecular Dynamics for Liquid Metals, *Phys. Rev. B* **47**, 1, 558-561.

10 Kresse G., Furthmüller J. (1996) Efficiency of *Ab-Initio* Total Energy Calculations for Metals and Semiconductors Using a Plane-Wave Basis Set, *Comput. Mater. Sci.* **6**, 1, 15-50.

11 Perdew J.P., Burke K., Ernzerhof M. (1996) Generalized Gradient Approximation Made Simple, *Phys. Rev. Lett.* **77**, 18, 3865-3868.

12 Perdew J.P., Burke K., Ernzerhof M. (1997) Errata: Generalized Gradient Approximation Made Simple [Phys. Rev. Lett. **77**, 3865 (1996)], *Phys. Rev. Lett.* **78**, 7, 1396.

13 Blöchl P.E. (1994) Projector Augmented-Wave Method, *Phys. Rev. B* **50**, 24, 17953-17979.

14 Kresse G., Joubert J. (1999) From Ultrasoft Pseudopotentials to the Projector Augmented-Wave Method, *Phys. Rev. B* **59**, 3, 1758-1775.

15 MedeA-Gibbs: Gibbs Licence IFPEN-CNRS-Université Paris-Sud.

16 MedeA: Materials Exploration and Design Analysis. Copyright© 1998-2012 Materials Design, Inc.

17 Boutard Y., Ungerer P., Teuleur J.-M., Ahunbay M.G., Sabater S.F., Pérez-Pellitero J., Mackie A.D., Bourasseau E. (2005) Extension of the Anisotropic United Atoms Intermolecular Potential to Amines, Amides and Alkanols: Application to the Problems of the 2004 Fluid Simulation Challenge, *Fluid Phase Equilib.* **236**, 1-2, 25-41. N_2: d_{NN} = 109.8 pm, d_{NX} = 54.90 pm, $q_N = -0.5075$, $q_X = 1.015$; CO_2: d_{CO} = 114.9 pm, $q_C = 0.6512$, $q_O = -0.3256$.

18 Jorgensen W.L., Chandrasekhar J., Madura J.D., Impey R.W., Klein M.L. (1983) Comparison of Simple Potential Functions for Simulating Liquid Water, *J. Chem. Phys.* **79**, 2, 926-935. H_2O: d_{OH} = 95.72 pm, $a_{HOH} = 104.52°$, $q_O = -0.834$, $q_H = 0.417$.

19 Chen L.-F., Soriano A.N., Li M.-H. (2009) Vapour Pressures and Densities of the Mixed-Solvent Dessicants (Glycols + Water + Salts), *J. Chem. Thermodyn.* **41**, 6, 724-730.

20 Bezus A.G., Kiselev A.V., Lopatkin A.A., Du P.Q. (1978) Molecular Statistical Calculation of the Thermodynamic Adsorption Characteristics of Zeolites Using the Atom-Atom Approximation. Part 1.-Adsorption of Methane by Zeolite NaX, *J. Chem. Soc., Faraday Trans. 2* **74**, 367-379.

21 Lachet V., Boutin A., Pellenq R.J.-M., Nicholson D., Fuchs A.H. (1996) Molecular Simulation Study of the Structural Rearrangement of Methane Adsorbed in Aluminophosphate $AlPO_4$-5, *J. Phys. Chem.* **100**, 21, 9006-9013. $q_{Al} = 1.60$, $q_P = 2.00$, $q_O = -0.90$.

22 Di Lella A., Desbiens N., Boutin A., Demachy I., Ungerer P., Bellat J.-P., Fuchs A.H. (2006) Molecular Simulation Studies of Water Physisorption in Zeolites, *Phys. Chem. Chem. Phys.* **8**, 46, 5396-5406.

23 Puibasset J., Pellenq R.J.-M. (2008) Grand Canonical Monte Carlo Simulation Study of Water Adsorption in Silicalite at 300 K, *J. Phys. Chem. B* **112**, 20, 6390-6397. $q_{Si} = 2.0$, $q_O = -1.00$.

24 Panagiotopoulos A. (1987) Direct Determination of Phase Coexistence Properties of Fluids by Monte Carlo Simulation in a New Ensemble, *Mol. Phys.* **61**, 4, 813-827.

25 Smit B., Karaborni S., Siepmann J.I. (1995) Computer Simulations of Vapor-Liquid Equilibria of *n*-Alkanes, *J. Chem. Phys.* **102**, 5, 2126-2140.

26 Darden T., York D., Pederson L. (1993) Particle Mesh Ewald: An N-log(N) Method for Ewald Sums in Large Systems, *J. Chem. Phys.* **98**, 12, 10089-10092.

27 Desbiens N., Demachy I., Fuchs A.H., Kirsch-Rodeschini H., Soulard M., Patarin J. (2005) Water Condensation in Hydrophobic Nanopores, *Angew. Chem. Int. Ed.* **44**, 33, 5310-5313.

28 Abrioux C., Coasne B., Maurin G., Henn F., Jeffroy M., Boutin A. (2009) Cation Behavior in Faujasite Zeolites upon Water Adsorption: A combination of Monte Carlo and Molecular Dynamics Simulations, *J. Phys. Chem. C* **113**, 24, 10696-10705.

29 Martín-Calvo A., Lahoz-Martín F.D., Calero S. (2012) Understanding Carbon Monoxide Capture Using Metal-Organic Frameworks, *J. Phys. Chem. C* **116**, 11, 6655-6663.

30 Dunne J.A., Mariwala R., Rao M., Sircar S., Gorte R.J., Myers A.L. (1996) Calorimetric Heats of Adsorption and Adsorption Isotherms. 1. O_2, N_2, Ar, CO_2, CH_4, C_2H_6 and SF_6 on Silicalite, *Langmuir* **12**, 24, 5888-5895.

31 Miller M.B., Chen D.-L., Xie H.-B., Luebke D.R., Johnson J.K., Enick R.M. (2009) Solubility of CO_2 in CO_2-philic oligomers: COSMOtherm Predictions and Experimental Results, *Fluid Phase Equilib.* **287**, 1, 26-32.

32 Weitkamp J., Puppe L. (1999) *Catalysis and Zeolites: Fundamentals and Applications*, Springer, New York, 1999.

33 Koros W.J., Fleming G.K. (1993) Membrane-Based Gas Separation, *J. Membr. Sci.* 83, 1, 1-80.

34 Caro J., Noack M., Koelsch P., Schaefer R. (2000) Zeolite Membranes – State of their Development and Perspective, *Micropor. Mesopor. Mater.* 38, 1, 3-24.

Final manuscript received in July 2012
Published online in March 2013